

# Ice Accretion on Wind-Turbines

Prof. Laszlo Fuchs<sup>1,2</sup> and Dr. Robert-Zoltan Szasz<sup>2</sup>

<sup>1</sup>) KTH, Royal Institute of Technology  
Valhallavägen 79, S-10044, Stockholm, *lf@mech.kth.se*, <sup>2</sup>) Lund University,  
Ole Römersväg 1, S-22100, Lund, *robert-zoltan.szasz@energy.lth.se*

**Abstract**—Ice deposition on the stationary parts and the blades of a wind turbine is modeled by a coupled Eulerian-Lagrangian approach. The influence of wind velocity profile and droplet size on the area of ice deposition is evaluated. The results show that most ice is deposited at the second third of the blades and on the frontal part of the tower. Neither the velocity profile or droplet size have significant influence the distribution of the deposited droplets.

## I. INTRODUCTION

Due to the decreasing fossil fuel resources there is an intensive research to find alternative energy sources. One promising possibility is the use of wind energy which has a further advantage that it does not contribute at all to the chemical pollution of the environment. The wind turbines used for the conversion of the kinetic energy of the wind to electricity are getting larger and larger. This size increase is associated with certain problems.

One of the major issues for wind turbines installed at places with cold climate is the deposition of ice on the turbine blades and on the tower. The deposited ice layer changes the shape of the blades profile and by this compromises the efficiency of the turbine in addition to the modified loading on the structure. To limit the cost of possible countermeasures, it is desired to predict the location where most ice is deposited. Ice accretion on wind turbines have been studied mainly empirically and a number of technical solution to the problem has been suggested. These techniques are based on different sensors in combination of measures to prevent/reduce ice accretion in a closed loop control manner. A recent review of ice sensors for wind turbines is given by Homola et al [6]. Altogether 29 different methods for detection of icing have been found, and these have been compared with respect to a list of some basic requirements for an icing sensor for wind turbine applications. The large number of approaches is an indicator to the fact that the authors [6] could not find reports of ice sensors performing satisfactorily. More systematic work has been made in recent years. Hochart et al [7] have carried out an experimental study by doing icing simulations on a 0.2 m NACA 63 415 blade profile in a refrigerated wind tunnel. The shapes and masses of the ice deposits were measured, as well as the lift and drag forces of the iced

profiles. The results show that when glaze or rime accreted on the blade profile, lift decreases and drag increases. Dalili et al [8] state that initial ice adhesion may slightly modify the original aerodynamic profile of the blade; continued ice accretion can drastically affect the structural loading of the entire rotor leading to potentially dangerous situations. Bose [9] and [10] carried out measurements of the shape changes of the turbine blade under glaze icing conditions. Further recent studies [11]-[14], report wind tunnel experiments of ice accretion. We have found it more difficult to find reports of computational modelling of the complex processes associated with ice accretion. The complexity stems from the fact that the outcome of the results strongly depends on coupled processes of mass and heat-transfer. These depend on the whether conditions but these are not well documented. In the following we report some initial steps that would lead to the prediction of ice accretion. We report the computation (LES) of the flow past a complete three bladed HAWT model. The air is assumed to contain water droplet which freeze on the solid object that they impact upon.

In the following, we present such a prediction tool based on a combined Eulerian-Lagrangian method. There are multitude of factors that influence the flow around a wind turbine, including incoming wind characteristics (e.g. vertical and horizontal variation turbulence characteristics), temperature distribution in space and time, geometrical changes due to variation in loading, etc. In this paper we investigate the influence of two of the parameters. First, the influence of the wind velocity profile is evaluated by comparing two cases with velocity profiles characteristic to stable and unstable conditions. Secondly, the influence of the droplet size is studied by comparing two cases where the droplet diameters differ by an order of magnitude.

## II. METHODS

A coupled Euler-Lagrange solver has been used to model ice accretion on the wind turbine blades. Only one-way interaction has been considered between the two phases, i.e., the water droplets are transported by the air, flow but they assumed not to perturb the flow field itself. When a droplet hits a solid surface it is assumed that the droplet freezes instantaneously on the same position.

A. Flow solver

The air flow has been computed by an incompressible Navier-Stokes solver based on finite differences. Third and fourth order schemes are used for the convective and diffusive parts, respectively. Turbulence is accounted for using Large Eddy Simulations (LES). The Immersed Boundary method (c.f. [2]) is used to account for solid surfaces. Further details of the flow solver are found e.g. in [3] and [5].

B. Particle tracking

The water droplets are modeled as small solid spherical particles transported by the air. The droplets are released every timestep, at a location at few blade diameters upstream of the wind turbine. All droplets have the same radius and density. The initial velocity of the droplets equals to the local air velocity, which is interpolated from the flow. After release, the droplets are transported by the air subject to a drag force,  $F_D$ , (Eq. 1):

$$F_D = 0.5\pi r^2 |U_C - U_D| (U_C - U_D) C_D \quad (1)$$

where  $r$  is the droplet radius,  $U_C$  the air (continuous phase) velocity,  $U_D$  the droplet velocity and  $C_D$  the drag coefficient. The droplets are tracked until one of the following events happens:

- The droplet hits the any part of the winds turbine
- The droplet exits at the side of the domain
- The droplets passes a prescribed axial position downstream (since we are interested only in the ice deposition, the computational effort is considerably reduced by eliminating the particles in the regions which are not interesting any more)

When a droplet hits the wind turbine its position and the time instance is logged for post-processing. Furthermore, instantaneous snapshots of droplet positions and velocities are saved with regular intervals for statistical analysis.

III. PROBLEM SET-UP

The flow field around a model three-bladed wind-turbine is computed (see Figure1)

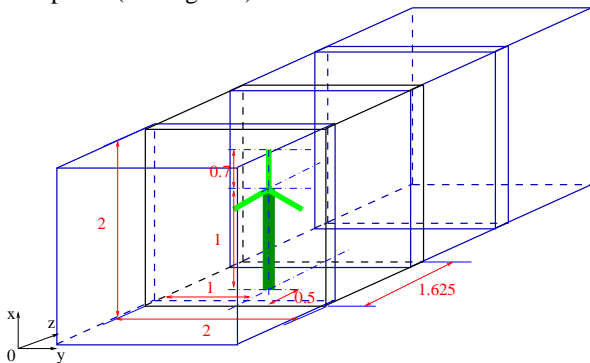


Fig. 1 Sketch of the computational domain and the coordinate system used herein.

The domain is divided into four blocks, these blocks being computed in parallel on four processors. Each block has the size of 2x2x1.625 units. The wind turbine is located in the second block, centrally in Y direction. The length of the blades is 0.7 units. At the inlet a constant wind profile has

been imposed according to equation (2):

$$w(x) = 0.2561317 \cdot x^m \quad (2)$$

where  $x$  is the height above the ground level and the exponent,  $m$ , indicates the stability of the atmospheric boundary layer. The angular speed of the turbine is fixed to 0.39 rot/s. At the outlet, flux conserving, zero gradient conditions are used. Previous tests [5] have confirmed that the zero gradient boundary condition does not disturb the solution close to the wind turbine.

Every time-step, 201x201 droplets are released, arranged uniformly over a rectangular area of 1.6x1.6 units, parallel to the turbine blades, located 0.1 units upstream the turbine tower, having the center on the rotation axis (Plane A in Figure 2). The droplets are tracked until an axial position of 0.1 units downstream the turbine tower (Plane B in Figure 2).

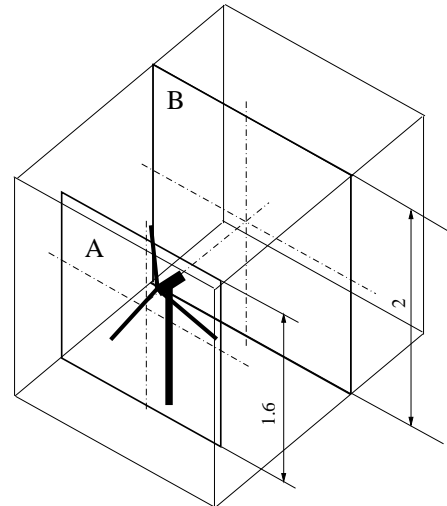


Fig. 2 Planes for the release of the droplets (A) and their elimination (B)

Three cases have been computed, summarized in Table 1. Case A is the base case and corresponds to an unstable atmospheric boundary layer profile and 0.5 mm radius droplets. To assess the influence of the wind profile, in Case B a stable atmospheric boundary layer profile has been considered. In order to evaluate the influence of droplet size, in the last case larger droplets were released (the wind profile being the same as in Case A). Each computation has been run for approximately twelve complete blade-rotations. During this period, more than 21 million droplets are deposited on the blades. This amount is considered to be adequate to obtain reliable statistical results.

TABLE I  
SUMMARY OF CASES

Case	$m$ (Eq. (2))	$r_{\text{drop}}$ (mm)
A	0.2	0.5
B	0.4	0.5
C	0.2	5

IV. RESULTS

In the followings the main features of the flow field will be summarized shortly, followed by a detailed description of the statistics related to the droplet transport.

A. Flow field characteristics

Figure 3 shows the average axial velocity field in cross-section through the tower, parallel to the wind direction. One can observe the wakes behind the turbine tower and the mast and generator house. At the positions corresponding to the tip vortices local maximum of the axial velocity field are seen. Due to the interaction of the tip vortices with the wake behind the turbine tower, at the lowest position of the blades tip the axial velocity has lower magnitude than the one corresponding one at the highest position. For the same reason, the wake downstream the tower is shorter at with distance from the ground.

An instantaneous snapshot of the vortices visualized by the  $\lambda_2$  method is shown in Figure 4. The large-scale spirals due to the tip vortices are clearly seen, as well as the wake behind the tower. Downstream the mast an elongated structure is seen which corresponds to the swirl induced by the turbine blades. Around the tip vortex spiral smaller structures are seen which mark the presence of secondary vortices.

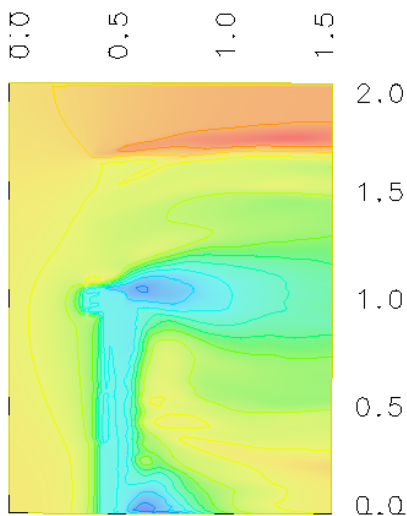


Fig. 3 Average axial velocity field in the mid-plane. Note the wake behind the mast and the generator house. One may also observe the effect of the horse shoe vortices that are formed by the mast at and close to the ground.

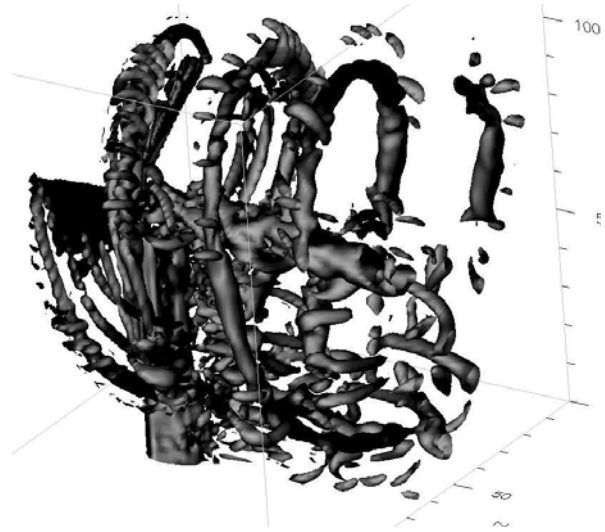


Fig. 4 Instantaneous vortices visualized with the  $\lambda_2$  method

B. Droplets depositing on the turbine

The positions of the droplets at the impact with the turbine have been logged during the computations. To restore the position relative to the blade, these positions have been rotated around the turbine axis, in opposite direction to the blade rotation. Figure 5 shows the distribution of the droplets depositing on the turbine blades for Case A. At the center of the turbine relatively low amount of droplets deposit due to the presence of the stagnation point. Most of the droplets are found to deposit around the second third of the turbine blades. No significant differences between the three evaluated cases.

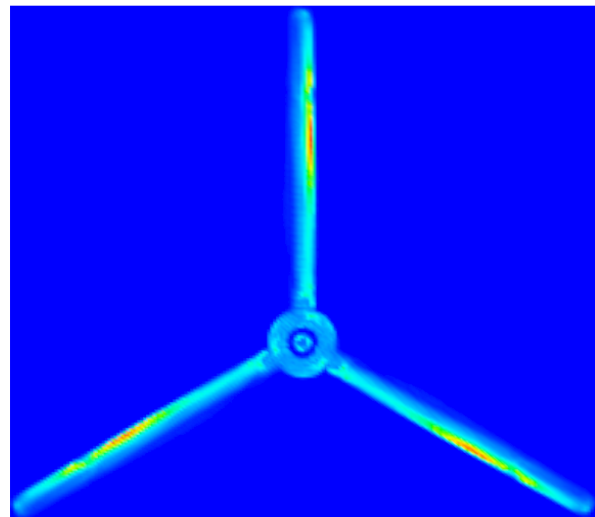


Fig. 5 Droplet number distribution on the blades. Case A. Most droplets are at the leading edge at about 2/3 of the blade span.

Figure 6 shows the radial distribution of the droplets deposited on the turbine blade at some locations. The distribution is normalized with the total number of droplets and the turbine axis corresponds to zero on the abscissa. Three peaks can be observed. The first from the left corresponds to the large concentration ring in the hub region. The second peak is located around the second third of the turbine blade which corresponds to the largest magnitudes shown in Figures

3-5 as well. In Figure 6 this peak is lower than the first one because all droplets are considered, thus a summation is carried out in azimuthal direction. The relatively steep gradient at the second peak is probably due to the geometry of the blade (twisted camber) possibly combined with grid resolution effects. No significant differences can be noticed among the cases.

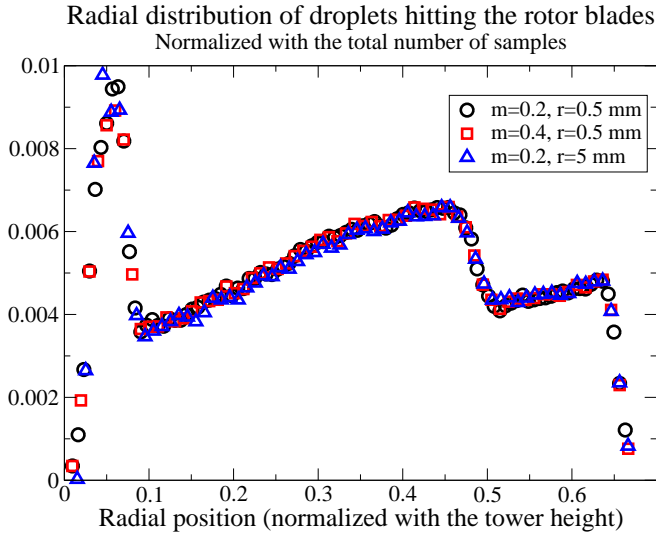


Fig. 6 Radial distribution of droplets hitting the turbine blade at some locations

Figure 7 shows the distribution of the droplets in azimuthal direction, here the angular position of the droplets is the one at the moment of impact (not corrected back to the blade position). One can observe a relatively uniform distribution of impact distribution, with a slight decrease of the number of depositing droplets at minus ninety degrees (position of the tower). Note that the scale on the ordinate which covers a rather short range.

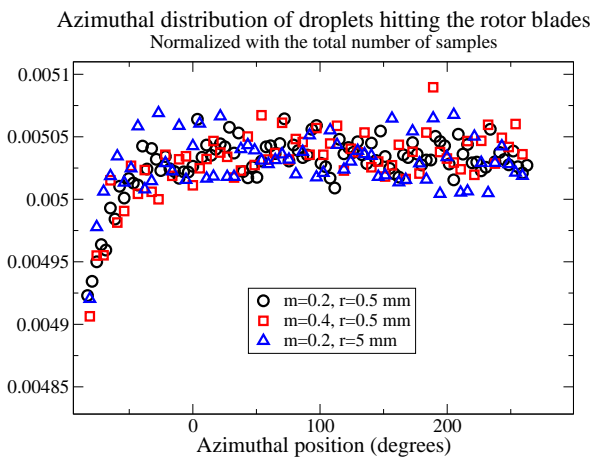


Fig. 7 Azimuthal distribution of droplets position hitting the turbine blade

C. Droplets hitting the tower

Beside the droplets depositing on the turbine, the ones

hitting the tower have been also logged during the computations. Figure 8 shows the time evolution of the number of droplets hitting the tower for the base case (Case A). To increase understanding, the histogram of the time history is shown. The total runtime has been divided in one thousand bins. In the figure (8) only a short time window is shown. The time on the abscissa is normalized with the number of complete rotations of the blades. One can observe a cyclic evolution of the amount of deposited droplets. The period corresponds to the blade passage frequency. As the blades are shading the tower, the number of droplets depositing decreases. When the tower is uncovered again, the number of droplets rises suddenly to the peak value.

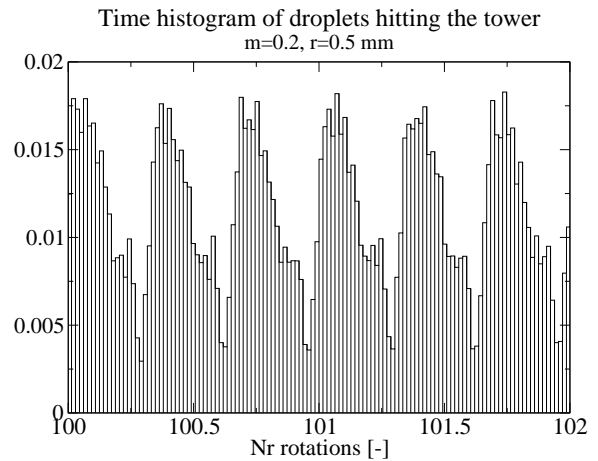


Fig. 8: Time distribution of the droplets hitting the tower. Case A.

The vertical distribution of droplets for the three studied cases is shown in Figure 9. The distributions for all cases have a bipolar character; most of the droplets are deposited around 75% of the tower height. The case with large droplets (blue line) has a more uniform distribution, the two maxima having almost the same magnitude. The cases corresponding to small droplet sizes are more asymmetric and almost no influence of the inlet velocity profile can be seen.

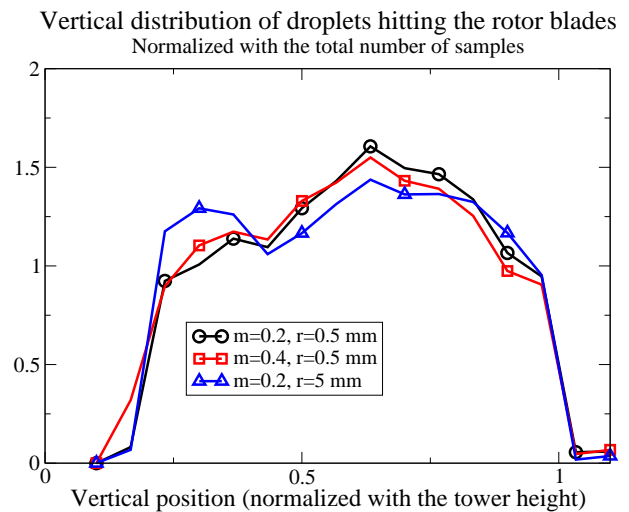


Fig. 9: Distribution of the vertical position of the droplets hitting the tower.

The horizontal (Figure 10) and axial (Figure 11) distribution of the droplets are strongly asymmetric, most of the droplets are deposition on the front- and right-hand-side of the tower. The influence of the droplet size and velocity profile is not significant.

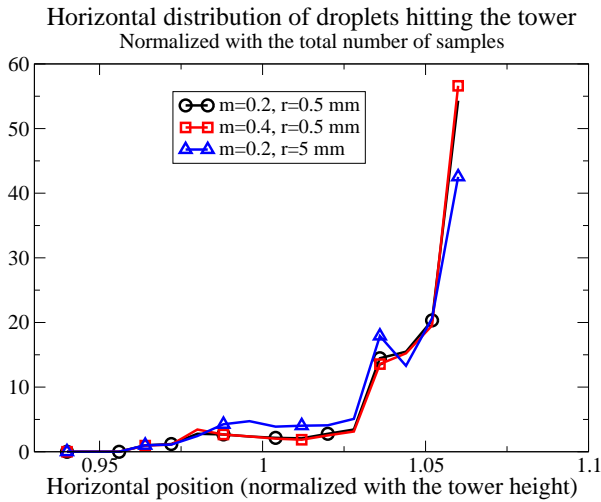


Fig 10 Distribution of the horizontal position of the droplets hitting the tower.

negligible influence, while the inlet velocity profile has a stronger effect. The same conclusions can be drawn looking at the vertical distribution of the droplets (Figure 13). The axial distribution of the droplets shows a decrease of the number of droplets at the position corresponding to the frontal part of the wind turbine, being constant further downstream (see Figure 14).

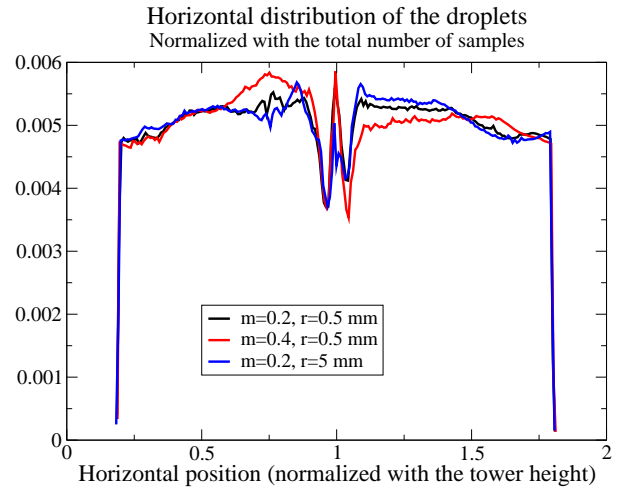


Fig. 12: Distribution of the droplets in horizontal direction

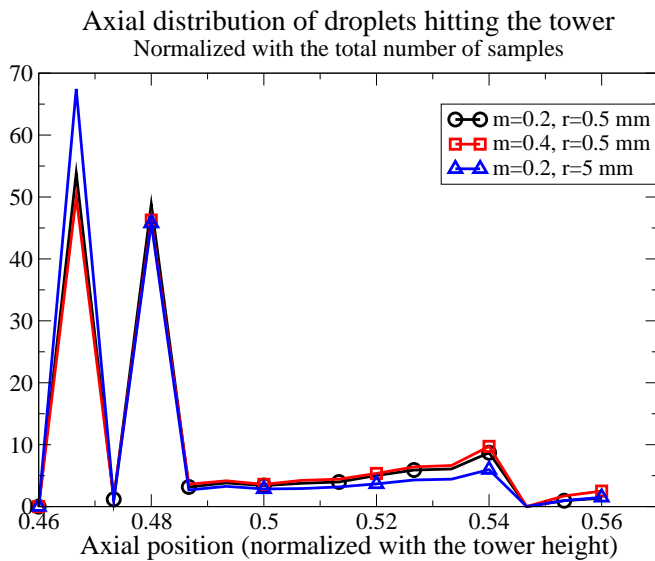


Fig. 11 Distribution of the axial position of the droplets hitting the tower.

The histogram of the vertical position (parallel to the tower) is shown in Figure 13 and the corresponding histogram of the axial position of the droplets (in the wind direction) is shown in Figure 14.

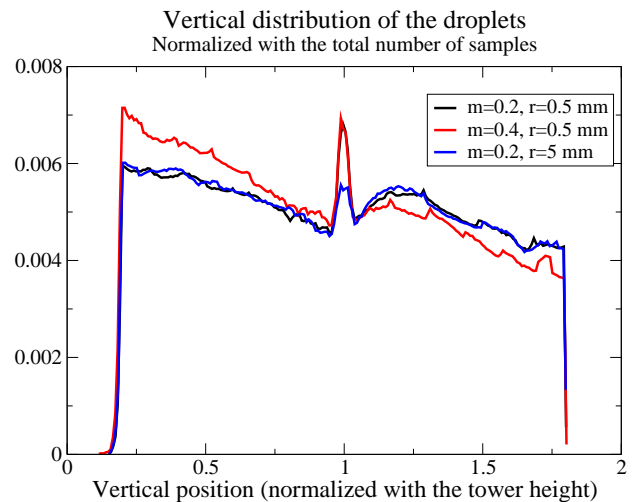


Fig. 13: Distribution of the droplets in vertical direction

#### D. Characteristics of the instantaneous discrete phase

The instantaneous position and velocity of the droplets before deposition has been saved periodically for post-processing analysis. The following figures show statistics of the droplets at the last saved time instance.

The histogram of the horizontal position (parallel to the turbine disc) is shown in Figure 12. The droplets positions have been distributed in 200 bins. The profiles are qualitatively similar, the droplet size is found to have

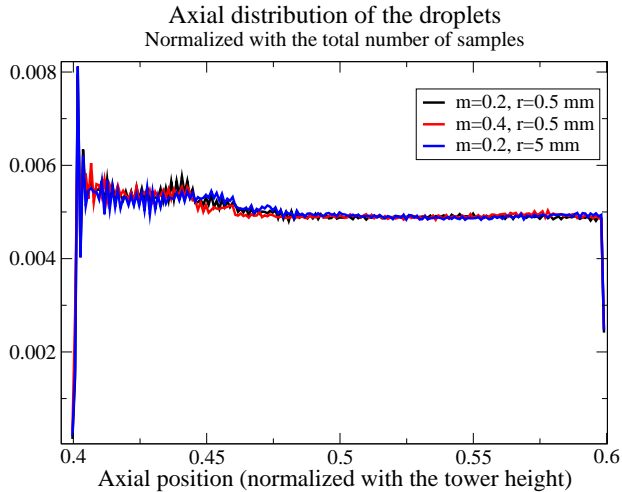


Fig. 14: Distribution of the droplets in axial direction

The histogram of the droplets vertical and horizontal velocity components are shown in Figures 15 and 16, respectively. Both distributions are centered around the origin. As seen, neither the inlet velocity profile or droplet size

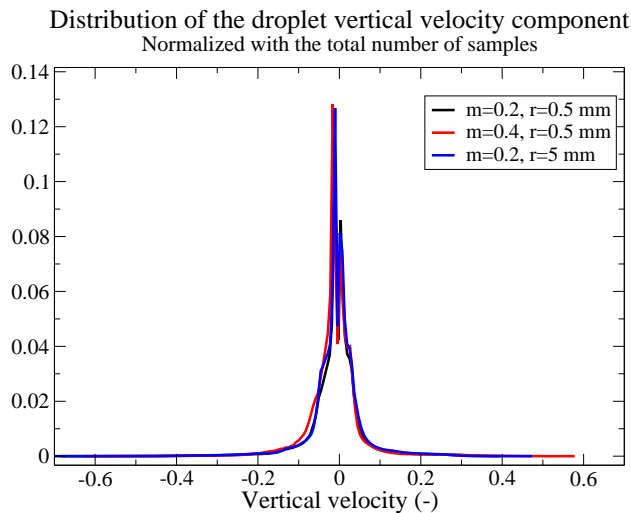


Fig. 15: Distribution of the droplet vertical velocity component

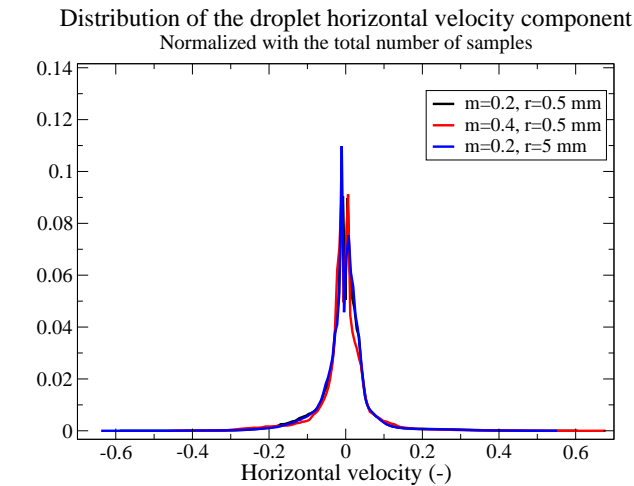


Fig. 16: Distribution of the droplet horizontal velocity component

The histogram of the droplets axial velocity component is shown in Figure 17. The size of the droplets has no significant influence, while the inlet velocity profile corresponding to the stable atmospheric boundary layer (red line) leads to a smoother distribution function, with fewer peaks than the cases with  $m=0.2$ . The local peak at the higher velocity region is at a higher speed for the stable profile. This is due to the fact the maximum flow speed is larger at the blade tip topmost position, thus the droplets will be accelerated more in this region than in the other two cases. Since for the stable velocity profile the magnitude of the velocity at the lowest blade position is less than for the unstable profile, the dominant peak is located at a smaller velocity magnitude.

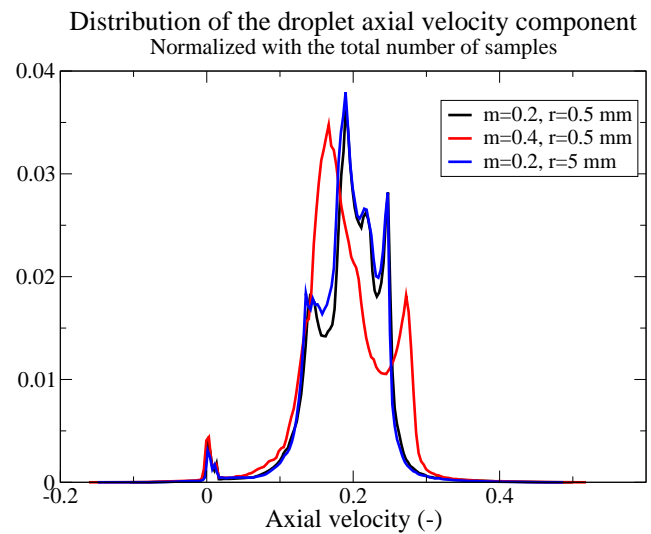


Fig. 17: Distribution of the droplet axial velocity component

The average axial velocity of the droplets at several axial positions is plotted for the three cases in Figure 18. In front of the turbine the droplets are accelerated initially, where after the average axial droplet velocity decreases due to blocking effect of the tower and the turbine blades. Behind the wind turbine the droplets velocities increase again asymptotically to the bulk velocity. Comparing Cases A (black) and B (red) one can observe that the stable velocity profile implies a lower average velocity of the droplets. In Case C (blue) the variations of the velocity magnitude are lower, as compared to the other two cases. The smoother velocity profile in Case C is due to the larger inertia of the large droplets.

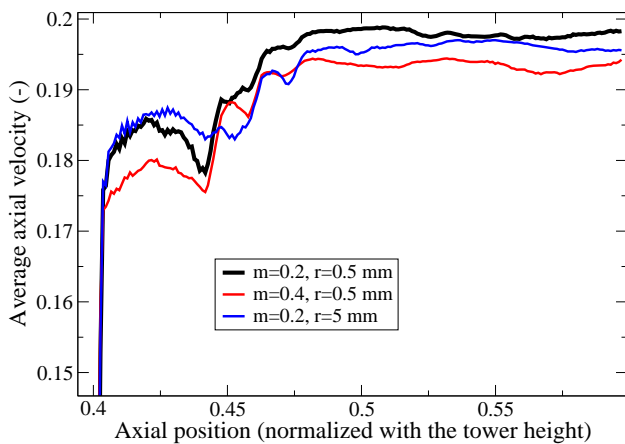


Fig. 18: Average axial velocity component of the droplets

The average vertical velocity of the droplets at several axial positions is plotted for the three cases in Figure 19. Again, the droplet size has almost no influence at all, while the inlet velocity

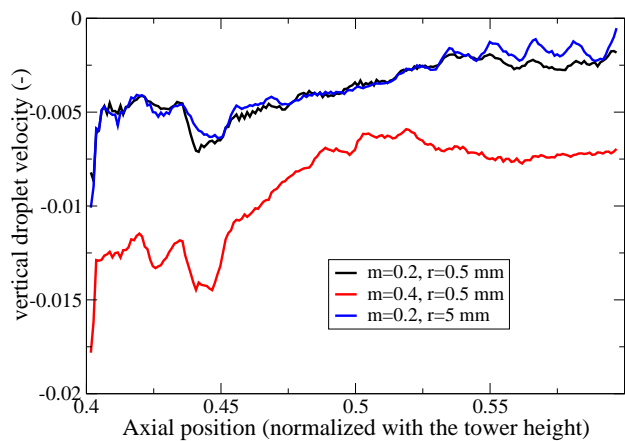


Fig. 19: Vertical component of the vertical droplet velocity

## V. CONCLUSIONS

Ice accretion on wind turbines has been considered by assuming that water droplet in the air stay on solid components of a complete wind turbine once they hit the sucha surface. The numerical approach uses LES for turbulence and a coupled Lagrangian-Eulerian for the droplets. Immersed Boundary method is used to handle the moving and stationary solid surfaces. Ice deposition is modeled by transporting water droplets and assuming that all droplets hitting the solid surfaces freeze immediately. Three cases have been computed to evaluate the influence of the wind velocity profile and droplet size.

The computations revealed that the evaluated parameters (mainly droplet size) had small influence on the deposition of the droplets on the turbine blades. In all cases most of the droplets are deposited around the second third of the blades.

The inlet velocity profile showed no significant influence on the number of droplets depositing on the tower, while

larger droplets had a smoother distribution over the tower height than the smaller ones. This is due to the inertia of the droplet that do not follow well the air-flow and thereby the distribution depends mainly on the initial (upstream) droplet distribution. Most droplets deposit around 75% of the tower height at the frontal and right-hand side of the tower.

The average of the droplets in the domain show small influence on the droplet position distributions, while the droplet velocity distributions and average velocity components at different axial positions showed a significant influence of the inlet velocity profile, but less influence of the inlet droplet size.

## VI. REFERENCES

- [1] van der Berg, G.P. Effects of the wind profile at night on wind turbine sound. *J. Sound and Vibration*, vol. 277, pp. 955-970, 2004.
- [2] Salewski, M., Duwig, C., Milosavljevic, V. and Fuchs, L. LES of Spray Dispersion and Mixing in a Swirl Stabilized GT Combustor, *AIAA paper*, AIAA-2007-0924, 2007.
- [3] Olsson, M. and Fuchs, L. Large Eddy Simulation of the Proximal Region of a Spatially Developing Circular Jet, *Phys. Fluids*, vol 8(8), pp. 2125-2137, 1996.
- [4] Gullbrand, J., Bai, X.S., Fuchs, L. High-order Cartesian grid methods for calculation of incompressible turbulent flows, *Int.J. Numerical Methods in Fluids*, vol 36, pp. 687-809, 2001.
- [5] Szasz, R.Z., Fuchs, L. Computations of the flow around a wind turbine: Grid sensitivity study and the influence of inlet conditions. Proc. Second International Conference on Turbulence and Interaction, TI2009, 2009
- [6] Homola, M.C., Nicklasson P.J., and Sundsbø, P.A. Ice sensors for wind turbines, *Cold Regions Science and Technology*, vol 46, pp. 125-131, 2006.
- [7] Hochart, C; Fortin, G; Perron, J, et al. Wind turbine performance under icing conditions. *Wind Energy*. vol. 11, pp. 319-333, 2008.
- [8] Dalili, N; Edrissy, A; Carriveau, R, A review of surface engineering issues critical to wind turbine performance. *Ren. & Sustainable Energy Rev.* vol. 13, pp. 428-438, 2009.
- [9] Bose, N. – Icing on small horizontal axis wind turbine 1: Glaze ice profiles. *J. Wind Engineering and Industrial Aerodynamics*, vol. 45, pp. 75-85, 1992.
- [10] Bose, N. – Icing on small horizontal axis wind turbine 2: 3-dimensional ice and wet snow formations. *J. Wind Engineering and Industrial Aerodynamics*, vol. 45, pp. 87-96, 1992.
- [11] Mayer, C; Ilinca, A; Fortin, G, et al. - Wind tunnel study of electro-thermal de-icing of wind turbine blades. *Int. J. Offshore and Polar Eng.* Vol. 17, pp. 182-188, 2007.
- [12] Wang, X; Bibeau, EL; Naterer, GF. Experimental investigation of energy losses due to icing of a wind turbine. *Int. Conf. on Power Engineering (ICOPE-2007); CHALLENGES OF POWER ENGINEERING AND ENVIRONMENT*, pp. 1143-1147, 2007.
- [13] Mayer, C; Ilinca, A; Fortin, G, et al. Wind tunnel study of the electro-thermal de-icing of wind turbine blades. 17th International Offshore and Polar Engineering Conference (ISOPE 2007); *PROCEEDINGS OF THE SEVENTEENTH (2007) INTERNATIONAL OFFSHORE AND POLAR ENGINEERING CONFERENCE*, pp. 693-699, 2007.
- [14] Battisti, L; Fedrizzi, R; Dal Savio, S, et al. - Influence of the type and size of wind turbines on anti-icing thermal power requirements for blades.. *EUROMECH Colloquium 464b on Wind Energy*, Conference CD, 2007.